Precipitate Effects on the Mechanical Behavior of Aluminum Copper Alloy: Part I. Experiments

H. SEHITOGLU, T. FOGLESONG, and H.J. MAIER

This article focuses on understanding the mechanical behavior of precipitation-hardened alloys by studying single and polycrystalline deformation behavior with various heat treatments. Aluminum-copper alloys are the focus in this work and their changing stress-strain behavior is demonstrated resulting from the different hardening mechanisms brought about by the various precipitates. Extensive transmission electron microscopy investigations facilitated the interpretation of the stress-strain behavior and the work hardening characteristics. The use of both single and polycrystals proved valuable in understanding the role of anisotropy due to crystal orientation *vs* precipitate-induced anisotropy. The experiments show that precipitation-induced anisotropy could offset the crystal orientation anisotropy depending on the orientation. This is clearly demonstrated with similar [111] and [123] behaviors under 190 °C and 260 °C aging temperatures. Experiments on pure aluminum crystals are also provided for comparison and understanding the crystal anisotropy in the absence of precipitates. Part I of this article will focus on experiments, and part II will describe the modeling of the effect of different metastable phases in the matrix acting as barriers to dislocation motion.

I. INTRODUCTION

PRECIPITATION-HARDENED alloys are a commercially important group of materials because their mechanical properties can be modified by heat treating and changing the microstructure. Precipitates introduced into the matrix interact with dislocations and affect their mobility, allowing control of the mechanical behavior of the material. Precipitate morphology, orientation, spacing, and degree of coherency with the matrix all contribute to the effectiveness of the precipitate as a barrier to dislocation motion. In addition, the mechanical behavior of a material can be influenced by its microstructure through processing steps during fabrication. These procedures can strengthen the original microstructure by refining the grain size. Orienting the grains in a particular direction can impact the mechanical behavior. To understand the causes of the changing mechanical properties of these materials, it is essential to characterize the microstructure and investigate the underlying deformation mechanisms.

The ease of plastic deformation depends on the crystallographic orientation of the material. However, a common microstructural feature of high-strength aluminum-copper alloys are plate-shaped precipitates that form on the cube faces of the fcc structure. These precipitates have an anisotropic contribution to the flow strength of the material such that crystallographically "soft" orientations are hardened by precipitates. In the first part of this series of articles, we will describe this anisotropy with experiments on single crystals of aluminum copper with selected orientations. Since the goal of this work is to develop a physically-based hardening law that can be incorporated into a polycrystal model and predict the stress-strain behavior through a variety of aging treatments, precipitate-induced anisotropy must also be accounted for in the work hardening description. The modeling is described in Part II of this series of articles.

The issues discussed previously are addressed in this work through mechanical experiments and microstructural analysis. The mechanical experiments are conducted under compression loadings at room temperature and the microstructural analysis involves transmission electron microscopy (TEM) of virgin and deformed samples and texture analysis for the polycrystalline cases. Ultimately, the research described in Part I of this series of articles links micromechanical deformation mechanisms with the macroscopic response. This understanding of the mechanical property-microstructure relationship is used in part II of this series of articles to develop a physically-based hardening description at the microscopic level that can be applied not only to the chosen materials but also to other precipitation-hardened alloys. The development of a comprehensive model that predicts the mechanical behavior of a precipitation-hardened alloy over a range of aging treatments is focused on in Part II.

II. MATERIALS BACKGROUND

A. *Materials Background*

A number of researchers have studied the mechanical behavior of aluminum and aluminum-copper alloys in both single-crystal and polycrystalline forms. The strain hardening behavior observed during the deformation of pure metals and alloys is generally attributed to obstacles in the material that impede or decrease the velocity of mobile dislocations. These interactions will be highlighted for aluminum and aluminum-copper in this work. We first review the deformation characteristics of each material as well as discuss the underlying deformation mechanisms and dislocation substructures responsible for plastic flow. Aluminum

H. SEHITOGLU, C.J. Ganthier Professor and Interim Head, is with the Department of Mechanical and Industrial Engineering, University of Illinois, Urbana, IL 61801. Contact e-mail: huseyin@uiuc.edu T. FOGLESONG formerly with the Department of Mechanical and Industrial Engineering, University of Illinois, Urbana, IL 61801, is Research Engineer, with Exxon Mobile Upstream Research Company, Houston, TX 77046. H.J. MAIER, Professor, is with the Department of Materials Science, University of Paderborn, D-33905 Paderborn, Gemany.

will be discussed first, followed by aluminum-copper alloys. The background provided here will be useful in understanding the current experimental results as well as in the development of a stress-strain response for precipitation-hardened aluminum.

B. *Aluminum Background*

Three stages of deformation are most commonly observed in aluminum single crystals starting with stage I, the easy glide stage. For aluminum at room temperature, the easy glide stage can account for up to 5 pct strain.[1] During this early stage of deformation, slip occurs only on the primary glide plane. Crystals that are oriented to activate more than one slip system from the onset of deformation will not produce a region of easy glide and will begin work hardening with stage II or stage III upon the onset of yielding.[1] The second stage of hardening also produces a nearly linear stress-strain curve, but the hardening rate is approximately 10 times greater than that of stage I. During straining in stage II, dislocations begin to tangle with one another and the common cell structure becomes more pronounced with increasing deformation. Lomer–Cottrell (LC)[2,3,4] locks are also commonly associated with stage II deformation as dislocations on intersecting (111) planes come into contact with one another and form sessile (stationary) dislocations. The increased hardening rate during this stage of deformation can be attributed to dislocation pileups at barriers such as LC locks and dislocation tangles or to glissile dislocations intersecting the sessile dislocations that traverse the slip plane. In most materials, these forest dislocations are present in the matrix as a result of material processing.

The final stage of hardening common to fcc metals is termed stage III, also commonly referred to as parabolic hardening because of the gradually decreasing rate of hardening.[5,6] This stage is less dependent on orientation than the previous two stages, but it is highly temperature dependent; the higher the temperature, the lower the flow stress that is required for the onset of stage III. The parabolic shape of the stress-strain curve and the decreasing hardening rate indicate the activation of relaxation mechanisms. It has been postulated that the onset of stage III indicates the breaking down or avoidance of the barriers that were formed during stage II, such as the LC locks.

The stacking fault energy (SFE) of the material also becomes a major factor in this third hardening stage as it dictates a material's ability to cross-slip. Materials with small stacking faults, resulting from a high SFE, such as aluminum (200 mJ m^{-2}), have lower strain hardening than materials with low SFE. This is because materials with high SFE can easily cross-slip and avoid obstacles. A detailed study of cross-slip in aluminum single crystals was performed by Cahn,[7] who investigated the cross-slip mechanism and its changing behavior with deformation and temperature. In addition, Kelly[5] examined the monotonic deformation of aluminum single crystals at room temperature and below. Cross-slip was observed at room temperature when the stress-strain curve became concave with respect to the strain axis at approximately 4 pct resolved shear strain. A number of researchers have considered the deformation of pure aluminum in order to understand the deformation mechanisms responsible for plastic flow of the material. Information has been gathered by examining the slip bands formed on the surface of the material in addition to analyzing the dislocation arrangements in the microstructure via TEM.[6,7–14] Considerable information can be obtained by interrogating the developing microstructure with TEM by *in-situ* studies and by tracking the changes in the microstructure during bulk deformation of the samples.

In pure metals, obstacles to continued dislocation motion are formed by the interactions between dislocations. For example, an obstacle can be presented in the form of a dislocation tangle or a cell wall, as discussed previously. Researchers have proposed a few different relationships to describe the flow stress of pure materials based on different dislocation interactions. The most commonly known relationship is the Hall–Petch relationship,[15,16] which describes an inverse square-root relationship between the flow stress and the grain size. A similar relationship, proposed by Bailey and Hirsch,[17] gave a proportional relationship between the flow stress and the total dislocation density. Basinski[18] presented another variation in which the flow stress is proportional to the density of forest dislocations as opposed to the total dislocation density.

C. *Aluminum-Copper Alloy Background*

The dislocation-precipitate interactions dictate the mechanical behavior of aluminum-copper alloys. The presence of precipitates in the aluminum matrix affects not only the critical shear stress required to initiate slip, but also the hardening behavior of the material. The degree to which these behaviors are affected depends upon the aging treatment used, which is directly responsible for the different precipitates. The generally accepted precipitation sequence in Al-Cu alloys[19,20,21] is supersaturated solid solution, Guinier–Preston (GP) zones, θ'', θ', and finally the formation of the stable θ phase.

The first metastable phase to form is the fully coherent GP zones, so named after their discoverers.[22,23] These zones are clusters of copper atoms that are plate like in shape, form on the {100} planes of the aluminum matrix, and are homogeneously nucleated in the matrix. They consist of sheets of Cu atoms up to 150 Å in diameter and only one or two atom layers thick.[24] Immediately after quenching from the solutionizing temperature, GP zones begin to nucleate at a very high rate with the rate decreasing with elapsed time. The rapid formation of GP zones after quenching is attributed to the "quenching-in" of excess vacancies,[24,25] which facilitate the formation of zones. The zones grow in such a manner as to minimize the rate of increase in strain energy of the precipitate and matrix.[26]

The second intermediate phase, θ'' (also referred to as GP II), is still coherent with the matrix, still resides on the {100} habit planes of the matrix, and is tetragonal in structure. This phase is a larger version of the GP zones and maintains the same chemical composition, hence the common reference to the phase as GP II. The maximum thickness of these platelets has been observed to be on the order of 100 Å with a diameter of 1500 Å.[27] The discrepancy in naming also arises from the fact that the phase has a defined tetragonal structure, which is argued to be more structured than a zone and as such should be termed a precipitate and have a distinct name. Byrne *et al.*[28] measured the separation

between the centers of the zones to be less than 150 Å for GP zones and less than 300 Å for θ''.

As the aging process continues, the final metastable precipitate to form is θ'. This precipitate is also tetragonal in structure but has a composition of $CuAl_2$. These precipitates are preferentially and heterogeneously nucleated on dislocations.[20,29,30] Associated with this preferential nucleation, if a planar dislocation arrangement is present in the material, then the precipitates will also initially nucleate in a planar arrangement.[20,30] The preference to nucleate on dislocations is because of the low interface energy, high elastic-strain energy of the precipitates, and the benefit of nucleating on dislocations in lowering the elastic strain energy.[31] The θ' precipitates have also been observed to nucleate on low-angle grain boundaries ($<$9 deg).[31] There have also been some instances in which θ' was observed to nucleate on high-angle grain boundaries.[32] The nucleation of θ' precipitates is independent of the GP zones and θ'', in that neither of these precipitates are necessary precursors to θ'. These precipitates are semicoherent with respect to the aluminum matrix as the broad faces of the precipitates are coherent with the matrix and the faces perpendicular to the habit plane are incoherent, with the misfit accommodated at the precipitate-matrix interface by dislocations that loop around the precipitates. After extended periods of aging, the broad faces of the θ' precipitates also begin to lose coherency and dislocations accommodate this misfit at the interface. The accommodation and coherency loss of θ' has been studied by a number of researchers.[33–41] In addition, the θ' precipitates also coarsen with increased aging due to the driving force of surface area reduction. The lengthening and thickening kinetics of the θ' plates have also been studied.[42,43,44] It should be noted that loads applied to the material during aging produce preferential nucleation on one or two of the three habit planes.[45–49] The effect of creep on the precipitation process has also been investigated.[50,51]

The final and equilibrium precipitate, θ, is body-centered tetragonal in crystal structure and is primarily incoherent with the matrix. Some coherency is left unless the precipitates are extremely large. The precipitates possess no single orientation relationship with the matrix and are no longer platelike in shape. The θ precipitate can be nucleated directly from the supersaturated solution if the aging temperature is high enough (*i.e.,* $>$300 °C) or even at lower temperatures if the kinetic and thermodynamic conditions in the material are favorable. However, at lower aging temperatures, if the general precipitation sequence is followed, θ will generally nucleate at planar boundaries, such as grain boundaries and at the interface of θ' with the matrix.[20,52] In general, θ nucleates on high-angle grain boundaries ($>$9 pct) because of its high surface energy, as the boundaries also have appreciable surface energy and can aid in lowering that of θ.[31] Laird and Aaronson[53] studied the formation of θ and observed the following three simultaneous reactions upon nucleation of θ: (1) θ consumes the θ' plates at which it nucleates, (2) regions of the matrix surrounding the θ precipitates simultaneously transform to θ, and (3) θ' plates in the vicinity of growing θ precipitates are dissolved. With extensive aging, the final microstructure will contain only θ precipitates that will continue to coarsen and will eventually be ineffective barriers to dislocation motion as their interparticle spacing becomes larger than the dislocation slip length.[54,55] Studies of the aging curves and the resulting precipitates have been completed by a number of researchers.[27,28,56,57]

D. *Mechanical Behavior of Aluminum-Copper Alloys and Precipitate-Induced Anisotropy*

Given the previous background on aluminum and aluminum copper alloys, it is worthwhile to review the role of precipitates on mechanical response and on anisotropy, which is the primary focus of this work. The slip and hardening behavior of aluminum alloys have been investigated by a number of researchers at different stages of the precipitation hardening process.[58–62] Very different slip behaviors have been observed depending upon the type of precipitate present in the matrix. These differences are more distinguished in single-crystal experiments where the crystal can be oriented for single slip. However, changes in the work hardening rate and the initial flow stress are still observed for polycrystal materials.

For material containing coherent particles, *i.e.,* GP zones or θ'', it has been found that the crystals deform in a similar manner to pure aluminum. These samples exhibit slightly higher work hardening rates than the pure material during initial flow. At small strains, these increased rates can be attributed to age hardening during straining, especially if the samples are being tested at room or elevated temperature immediately after quenching from the solutionizing temperature. At larger strains, the higher work hardening rates may be attributed to the lower stacking fault energy of the alloy than the pure material. The slightly higher yield stress of the material containing coherent particles is ascribed to a combination of the shearing of particles by dislocations resulting in atomic scrambling and local coherency strains near the GP zone that must first be overcome by the dislocation.[28,61] Gerold and Haberkorn derived an expression for the increase in the critical resolved shear stress as a result of coherent particles based on the interaction of edge dislocations with the coherency strain fields of the particles.[63]

Crystals containing thicker and more widely spaced particles that are semicoherent or completely incoherent with the matrix, *i.e.,* θ' or θ, exhibit relatively low initial yield stresses but work harden very rapidly. At the onset of plastic flow, the yield stress for materials containing θ precipitates is lower than that of the material containing the coherent precipitates because the precipitates are spaced further apart and the dislocation sources can initially operate with little hindrance; thus, yielding is relatively easy. Dislocations can no longer shear the precipitates because the particles are either semicoherent or incoherent with the matrix. Instead, they must bypass these obstacles often hypothesized by the Orowan looping mechanism. As plastic deformation continues, Orowan loops accumulate and are stored around the precipitates, thereby creating internal stresses. This accumulation of dislocations and the subsequent dislocation-precipitate interactions introduces a second component of hardening to the normal dislocation-dislocation interactions observed in the pure matrix material. The initial buildup of the dislocations around the particles results in the initially high work hardening rates for the material. The stresses oppose the activation of dislocation sources and interact heavily with mobile dislocations, resulting in the activation

of more than one slip system. As deformation continues, the stresses around the precipitates are alleviated by relaxation mechanisms that cause a steady-state number of loops around the precipitate.[60,64]

There have been some discrepancies on the exact nature of slip during deformation of single crystals with semicoherent and incoherent precipitates. Price and Kelly[61] attributed the observed rapid work hardening in tension to multiple slip. They did not observe a change in orientation or cross-section shape during straining. They considered that the multiple slip resulted because dislocations were forced to move on secondary slip planes by cross-slip or by rapid hardening on the primary plane. However, Russell and Ashby[60] found no evidence of extensive secondary slip in crystals oriented away from the edges of the stereographic triangle (similar orientations to those observed in Reference 61). They instead concluded that their samples deformed predominantly by primary slip. Russell and Ashby explained their results based on the crystals deforming as plastically nonhomogeneous materials,[64] and the observed rapid hardening was because of the accumulation of both statistically-stored and geometrically-necessary dislocations. Koda *et al.*[65] observed three types of dislocation-precipitate interactions with the θ' precipitates: (1) dislocation pileups against the precipitates; (2) dislocations adhered to the precipitate, *i.e.,* part of the dislocation line appeared to be embedded in the precipitate; and (3) dislocations held up between precipitates.

Single crystals containing GP zones or θ'', oriented for single slip, deform *via* the single system for much of the deformation, and the rate of hardening is similar to that of pure Al.[28,29] However, with the introduction of θ' or θ, multiple systems are now operative immediately upon yielding and the work hardening rates are initially high (on the order of $G/10$) saturating after a few percent strain.[28,29] These differences in slip operation can be distinguished not only by the shape of the stress-strain curve, but also by observing the slip steps on the surface of the crystal and the change in shape of the sample. For example, samples deforming by single slip with coherent precipitates exhibit long slip lines on the surface of the crystal, and a change in shape of the crystal occurs due to the geometric constraints imposed on the sample when deforming in single slip. For a crystal oriented for single slip that is forced to deform *via* multiple slip because of the presence of unshearable precipitates, the slip lines will be difficult to observe and the sample will not show significant shape change.[1,28,29]

In order to accurately model the effect of precipitates on the flow response of aluminum-copper alloys, it is also important to understand the concept of precipitate-induced anisotropy. When precipitates are introduced into the matrix, they reduce the flow anisotropy typical of single crystals or textured polycrystals. This is most readily apparent with the θ' precipitate. This phenomenon is also partly responsible for the Bauschinger effect in cyclic deformation. The mechanisms responsible for the buildup of a back stress are also responsible for precipitate-induced anisotropy in monotonic flow behavior. An aluminum alloy containing semicoherent, θ' precipitates exhibits the greatest Bauschinger effect.[58,59,62] By the Orowan theory, back stresses at the particles continue to accumulate during forward flow and subsequently produce a large Bauschinger effect upon reverse loading as they aid yielding in the reverse direction. The Bauschinger effect due to coherent precipitates[58,62] is relatively small and is similar to that observed in pure aluminum.[66]

The anisotropy attributed to the presence of precipitates is dependent upon not only the aging treatment but also the orientation of the crystal, for both single crystals and textured polycrystals. Moan and Embury[59] investigated the orientation dependence of the back stress for an aluminum-copper alloy and found that the back stress was greatest for crystals oriented for single slip and least for those oriented for multiple slip. The back stress is reduced in multiple slip orientations because it is possible for the slip systems to interact and form prismatic dislocation loops, which substantially lower the back stress.[59] Therefore, the stress-strain curve of a single crystal oriented for single slip would be comparable, in yield and work hardening, to that of a crystal oriented to activate multiple slip systems.

Barlat and Vasudévan[67] attempted to isolate the effects of precipitates on the anisotropy behavior by creating samples out of an aluminum alloy sheet that had the same grain size, isotropic crystallographic texture, and uniaxial yield strength after heat treating to either a under- or overaged conditions. They found that the different precipitates in the microstructure did have an impact on the anisotropy and that these changes could not be predicted by the original form of the Taylor–Bishop–Hill model.

III. EXPERIMENTAL PROCEDURE

A. *Material and Sample Preparation*

The materials chosen for this work were pure aluminum and an aluminum-4 wt pct copper alloy. The pure aluminum was representative of high SFE materials. The binary aluminum-copper alloy was used as the model precipitation-hardened alloy. The matrix material of the alloy was included in this work so that the effects of precipitates on the deformation mechanisms and resulting microstructures could be clearly distinguished, when compared with those of the matrix. Single crystals were chosen to eliminate the complicating effects of grain boundaries on the deformation mechanisms, highlighting the impact of orientation and precipitates on the mechanical behavior of the material. Compression experiments were conducted on these two materials for both single- and polycrystalline samples. The microstructures of deformed single- and polycrystal samples were analyzed by TEM to examine the dislocation-dislocation interactions of the aluminum material as well as the dislocation-precipitate interactions of the Al-Cu alloy.

The polycrystal compression samples were cast from 99.9 pct pure aluminum and 99.9 pct pure copper pellets in the Solidification Processing Laboratory, University of Illinois. The ingots were approximately 76.2 mm in length with a cross section of 25.4×25.4 mm after solidification and machining. The solidification microstructure, as determined by chemical etching, consisted of large directional grains on the order of 4 to 5 mm. Both materials underwent deformation and recrystallization to refine the grain size and to produce a more equiaxed grain distribution.

For recrystallization, the larger ingots were machined in half to yield large compression specimens of approximately $38.1 \times 25.4 \times 25.4$ mm. These specimens were compressed

to a strain of approximately 40 pct. The ends of the specimens were well lubricated with grease and TEFLON* sheets to reduce friction between the sample ends and the compression platens. These deformed specimens were then machined into the final compression sample size of $5 \times 5 \times 9$ mm.

*TEFLON is a trademark of Dupont, Wilmington, DE.

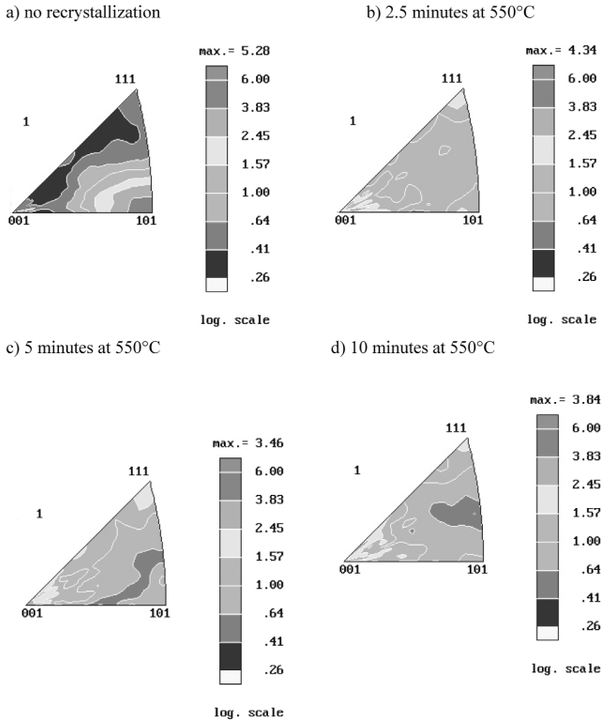

Fig. 1—Inverse pole figures tracking the texture changes with increasing recrystallization time at 550 °C: (*a*) no recrystallization, (*b*) 2.5 min, (*c*) 5 min, and (*d*) 10 min.

Table I. Summary of Crystallographic Orientations for the Pure Aluminum and Aluminum-4 wt pct Copper Alloy

Material	[111]	[117]	[123]	[112]
Pure Al	X	X	X	—
Al-4 wt pct Cu	X	X	X	X

To determine the appropriate recrystallization time for the aluminum and aluminum-copper samples, texture measurements were performed along with optical microscopy examinations of the grain morphology. Before compression and the recrystallization procedure, ingots were solutionized at 535 °C for 24 hours. The texture of a sample after heavy deformation and before recrystallization was first obtained as a baseline. Samples were then recrystallized at 550 °C for 2.5, 5, and 10 minutes, for the Al-4 pct Cu samples, and texture measurements were recorded. The inverse texture plots for these samples are given in Figure 1, with the texture shown in relation to the compression axis. It can be clearly seen that the heavily deformed sample before recrystallization exhibits a strong [101] texture that would be expected of a sample deformed by compression. Optical examination of this sample showed flattened and elongated grains. All three of the subsequent recrystallization times resulted in similar pole figures displaying, for the most part, randomly oriented grains with a slight preferential orientation of some grains at the [100] and [111] poles. The recrystallization time for the remainder of the polycrystal samples was chosen to be 5 minutes after inspection of the grains by optical microscopy. The sample recrystallized for only 2.5 minutes still displayed some elongated grains, while the 5- and 10-minute samples both contained equiaxed grains.

The single crystals were grown at Tomsk University (Russia) in an inert He environment using the Bridgman technique. The bulk single crystals were 30 mm in diameter and approximately 127 mm in length. Upon solidification, the bulk crystals were solutionized at 535 °C for 24 hours. Laue back diffraction was used to determine the orientation of the bulk crystals. After the orientation of the crystals had been determined, compression samples with a given crystallographic orientation were machined by spark erosion.

The crystallographic orientations chosen for each material are shown in Table I and the Schmid factors corresponding to the 12 fcc slip systems are given in Table II. The respective locations of the orientations within the stereographic triangle are depicted in Figure 2. Orientations were chosen that would exhibit varying degrees of slip system activity according to the Schmid law. The orientations at the corners of the triangle have multiple slip systems that are equally favored from the onset of deformation. Those on the

Table II. Schmid Factors (SFs) for Slip on the 12 Fcc Slip Systems for the Orientations given in Table I

Slip Direction	Slip Plane	[111]	[117]	[123]	[112]
[0,1,−1]	(1,1,1)	0	−0.43	−0.17	−0.27
[−1,0,1]	(1,1,1)	0	0.43	0.35	0.27
[1,−1,0]	(1,1,1)	0	0	−0.17	0
[0,1,1]	(−1,1,−1)	−0.27	−0.45	−0.29	−0.41
[1,0,−1]	(−1,1,−1)	0	0.34	0.12	0.14
[−1,−1,0]	(−1,1,−1)	0.27	0.11	0.17	0.27
[0,1,−1]	(−1,1,1)	0	−0.34	−0.12	−0.14
[1,0,1]	(−1,1,1)	0.27	0.45	0.47	0.41
[−1,−1,0]	(−1,1,1)	−0.27	−0.11	−0.35	0.27
[0,1,1]	(1,1,−1)	0.27	−0.32	0	0
[1,−1,0]	(1,1,−1)	0	0	0	0
[1,0,1]	(1,1,−1)	0.27	−0.32	0	0
Greatest SF		0.27	0.45	0.47	0.41

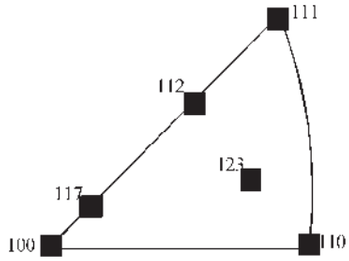

Fig. 2—Stereographic triangle showing the relative locations of the single crystals.

Table III. Aging Treatments for Single- and Polycrystal Al-4 wt pct Cu

Aging Treatment and Times	Single Crystal	Polycrystal
Natural aging	X	X
190 °C, 3 h	X	X
190 °C, 10 h	X	X
190 °C, 24 h	X	X
260 °C, 3 h	X	X
260 °C, 5 h	X	X
260 °C, 24 h	X	X

boundaries deform *via* double slip, and those on the interior of the triangle initially deform on only one slip system.

The aging treatments for the Al-Cu alloy were selected to provide microstructures with different precipitates and interparticle spacings by adjusting the aging temperature and time period. Two elevated aging temperatures were chosen, 190 °C and 260 °C, with aging times ranging from 3 to 24 hours, as listed in Table III. Most, but not all, of these heat treatments were conducted for every orientation. The resulting microstructures and precipitate spacings were analyzed by TEM and further information can be found in Foglesong's Ph.D. thesis.[68] Upon completion of aging, samples were quenched from the aging temperature in ambient temperature water.

One set of samples was not artificially aged at elevated temperature but remained at room temperature for more than 24 hours before testing. At room temperature, GP zones nucleate and alter the material properties with stabilization reached after 24 hours. To obtain an "as-solutionized" sample, the specimen must be stored cryogenically immediately upon quenching. The "solutionized" condition was not studied in this work.

B. *Mechanical Testing*

All of the experimental data were obtained from compression tests performed on rectangular samples with dimensions of $9 \times 5 \times 5$ mm and were performed in the Advanced Materials Testing Laboratory, University of Illinois. The experiments were conducted on a servo-hydraulic Instron load frame *via* an Instron controller (Instron, Canton, MA) through a LabVIEW interface. All of the compression tests were performed in displacement control, resulting in strain rates in the range of 10^{-4} to 10^{-5} s^{-1}. Strain was measured directly on the sample using a miniature MTS extensometer with a 3-mm gage length, as shown in Figure 3.

In uniaxial compression experiments, sample end effects can have an impact on the stress-strain behavior and measures were taken to minimize the end effects during the compression experiments of this study. Steps were taken to ensure that the specimen surfaces and compression platens were parallel. Friction effects at the specimen surface can also affect the modulus as a result of premature yielding at or near the sample ends. TEFLON tape and grease were placed between the two surfaces to minimize the friction stresses between the sample surface and compression platens. In addition, the sample surfaces were also smoothed and polished, to reduce the effects of friction.

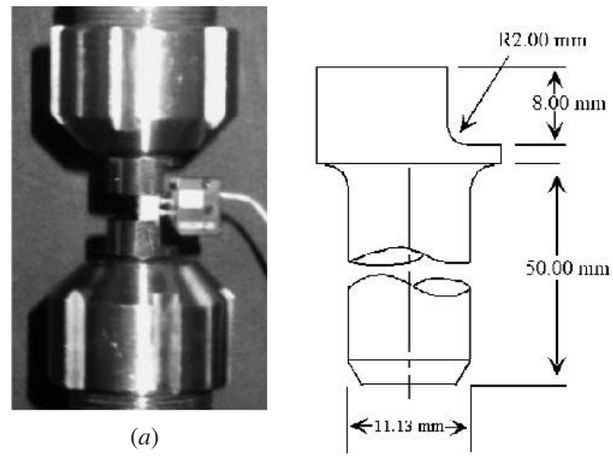

Fig. 3—(*a*) Experimental setup for the room-temperature compression experiments for single-crystal and polycrystal specimens and (*b*) schematic of compression platens with cutout for positioning of the miniature extensometer.

C. *Microstructural Analysis Techniques*

Transmission electron microscopy was performed using a PHILIPS* CM 200 electron microscope operated at 200 kV.

*PHILIPS is a trademark of Philips Electronic Instruments, Mahwah, NJ.

Representative single-crystal and polycrystal samples were examined at each aging treatment after compression testing. This approach permitted determination of the precipitates present in the materials and allowed an investigation of the resulting dislocation interactions with one another and with the precipitates.

The TEM samples were prepared by first machining slices approximately 1-mm thick from the bulk compression tested samples, using a low-speed saw. The slices were then mechanically ground using SiC paper, of progressively smaller grit size, followed by polishing with diamond paste, to a thickness of approximately 150 μm. The center of the TEM sample was preferentially thinned by dimple grinding with diamond paste, again in steps of progressively smaller diamond particle size. The electron-transparent area was generated by ion milling, and the sample holder was cooled by liquid nitrogen to minimize sample heating.

Texture analysis of the polycrystal samples was performed using a PHILIPS X'Pert X-ray diffraction machine operating at 45 kV and 40 mA using a Cu K_α source. A crossed-slit collimator was used as the primary optics with a slit width of 2×2 mm. The samples were mounted on the goniome-

ter stage with the compression axis of the specimen initially parallel to $\phi = 0$ deg. Measurements were taken at 5 deg increments as the goniometer was rotated through $\phi = 0$ to 360 deg and $\psi = 0$ deg to 85 deg. Pole figures were obtained for the (111), (200), and (220) poles and inverse pole figures were generated from these data using popLA software.[69]

IV. RESULTS

The experiments, microstructural observations, and modeling results cover a wide range of heat treatments that determine the initial microstructure and influence the resulting mechanical behavior. For this reason, the TEM observations will be discussed first as they provide a basis for analyzing and comparing the compression testing results across different orientations and heat treating conditions. A discussion of the results from the pure aluminum and aluminum-copper alloy single-crystal and polycrystal room-temperature compression experiments will follow. A comparison of the modeling simulations, generated with the VPSC model, for the single-crystal and polycrystal experimental results, is given in Part II.

A. *Microstructural Analysis*

Transmission electron microscopy was used to study the microstructures of the samples after various heat-treatment conditions. Because of the limited supply of single crystals, the samples were analyzed upon completion of the room-temperature compression tests. These images not only provided information concerning the resulting microstructure after the heat treatments but also gave insight into the interactions of the dislocations with one another and with the precipitates. One primary orientation was chosen to analyze the changing microstructure with subsequent heat treatments of the aluminum-copper single crystals. A relationship between the resulting precipitates and the time and temperature of the heat treatment was established to provide a basis for the subsequent modeling work.

For the pure aluminum, three single-crystal orientations ([123], [117], [111]) were chosen to study the resulting dislocation microstructure after room-temperature compression. For brevity, only the [123] TEM results are discussed in detail as subgrains were observed in all three orientations and the microstructures were similar to one another.

The [123] orientation was compressed to a strain of 9 pct and the resulting deformation substructure was comprised of subgrains, as shown in Figure 4(a). The subgrains were easily distinguished from true grains by tilting the TEM foil and noting the contrast. The average subgrain size, as determined by the linear intercept method, was 2.6 ± 0.9 μm, in good agreement with values reported in other works that have studied the substructures of deformed aluminum.[11,70,71] A magnified view of the dislocation network forming a subgrain boundary is shown in Figure 4(b).

The TEM viewgraphs for the Al-Cu under the 190 °C treatment and the no aging treatment are shown in Figures 5(a) and (b), respectively, the latter diffraction pattern verifying the presence of GP zones. In the case of 190 °C, 3-hour and 190 °C, 10-hour treatments, platelike structures characteristic of θ' precipitates are noted in Figures 6(a) through (c). Individual precipitate spacings were obtained after tilting the foil such that the precipitates were seen edge-on. From these data, average interparticle spacing was calculated using the method described in detail in Reference 72 and used in Part II of this series of articles. The emergence of small incoherent precipitates becomes apparent for the 260 °C, 3-hour treatment (Figures 7(a) through (c)). Both θ' and stable θ precipitates are noted for the 260 °C, 10-hour treatment shown in Figures 8(a) and (b). We note that θ maintains some coherency with the matrix. With respect to stress-strain response, however, this effect is negligible, and in the following, θ will simply be referred to as an incoherent precipitate.

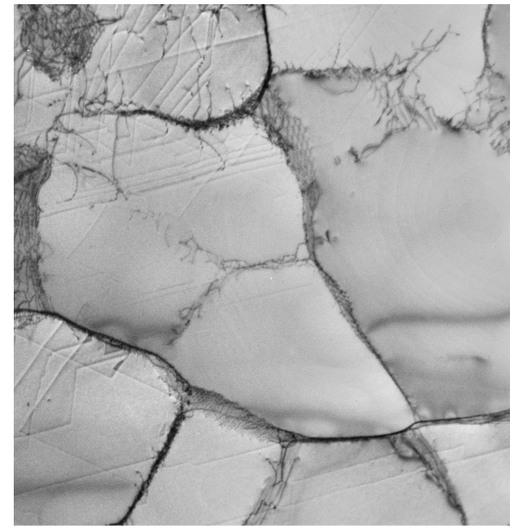

(*a*)

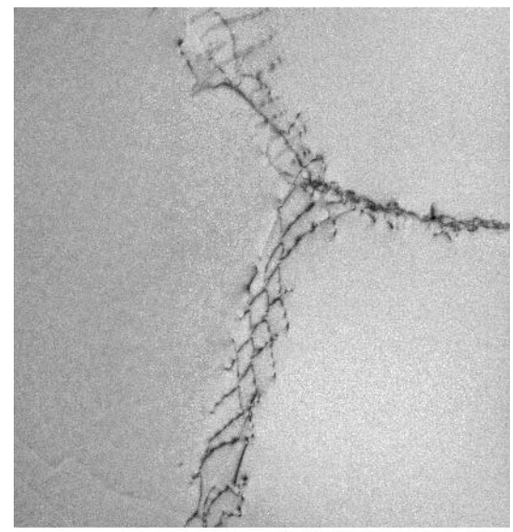

(*b*)

Fig. 4—(*a*) Pure aluminum single crystal, [123] orientation, showing the formation of subgrains at room temperature and (*b*) high-magnification view showing the dislocation network of a subgrain.

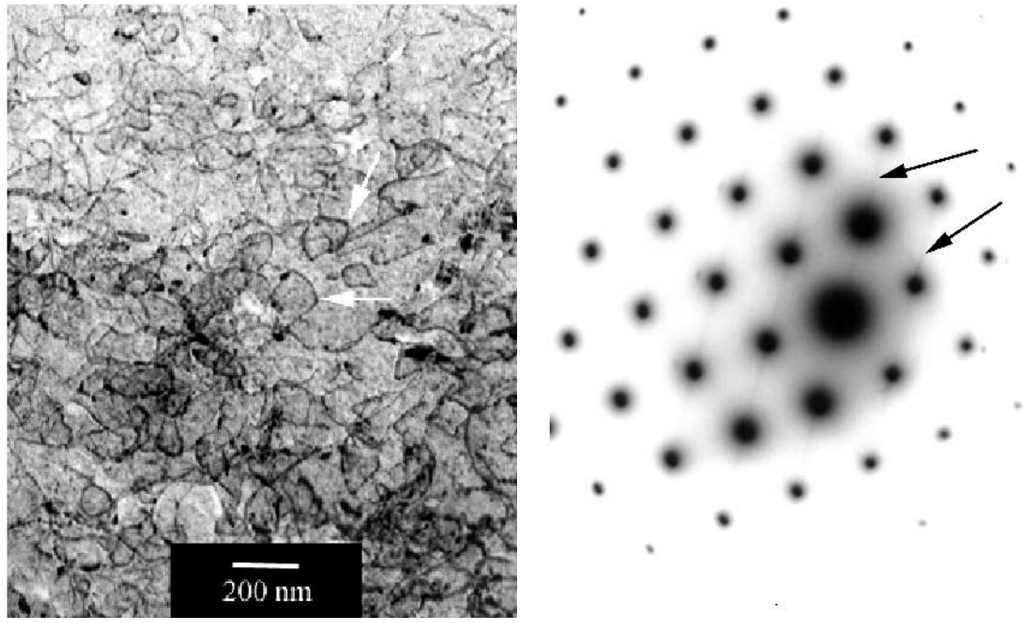

(*a*) (*b*)

Fig. 5—(*a*) Weak beam image of a single-crystal sample of Al-4 wt pct Cu in [112] orientation aged at 190 °C for 3 h. Contrast of this image has been reversed for ease of comparison. (*b*) Overexposed selected area diffraction pattern from a no aging [111] oriented single crystal verifying the presence of GP zones, as shown by streaks radiating from matrix reflections.

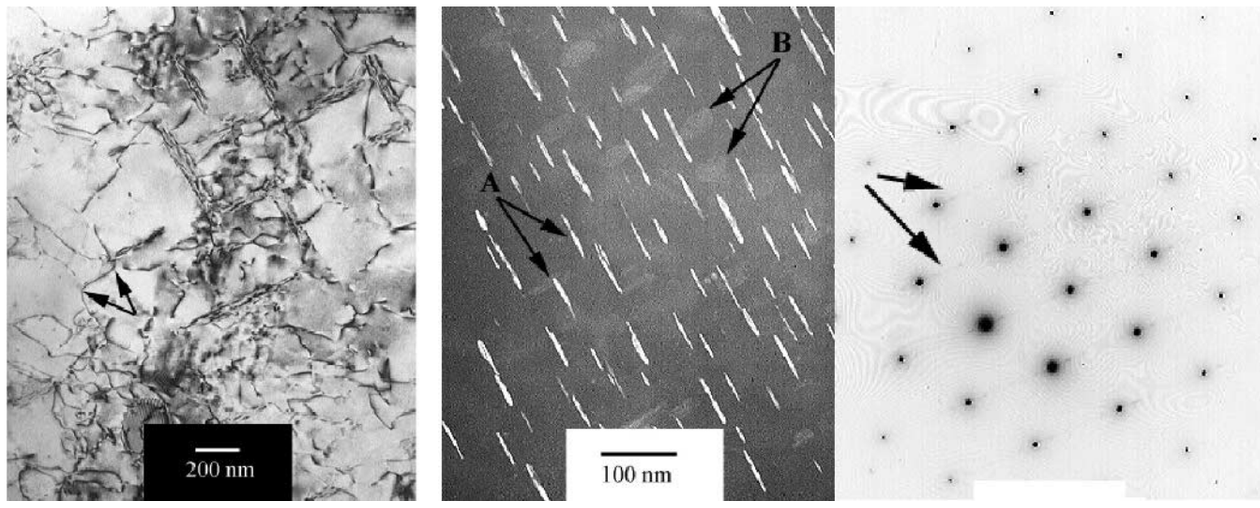

(*a*) (*b*) (*c*)

Fig. 6—(*a*) Two-beam bright-field image of a polycrystal sample of Al-4 wt pct Cu aged at 190 °C for 3 h showing possible evidence of small plate like precipitates due to 90 deg bending of some dislocations. (*b*) Polycrystalline sample aged at 190 °C for 10 h, conventional dark-field image clearly showing the θ' precipitates. (*c*) SAD pattern displaying streaks from precipitates.

B. *Mechanical Behavior*

The pure aluminum stress-strain (engineering) curves in compression are compared in Figure 9 for both the polycrystalline and single-crystal cases. The results reflect the flow anisotropy attributed to crystallography with [111] having the highest flow stress and highest strain hardening. The [111] has six favorably oriented slip systems, while initially, [117] and [123] have only two and a single active slip systems, respectively. The formation of dislocation cells or subgrains controls the work hardening in all these cases. The [111] orientation exhibits the lowest Schmid factor (0.27) and the highest interaction of slip systems producing the highest hardening.

The experimental stress-strain curves in compression are summarized in Figure 10 to illustrate the precipitation-induced anisotropy effect. Only the results for the [111] and

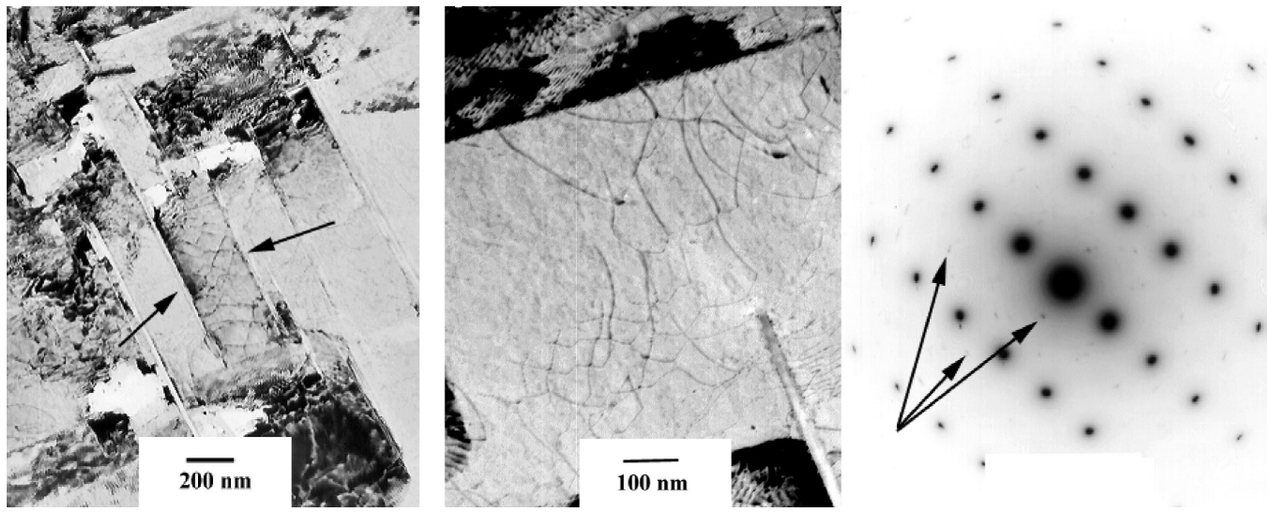

(*a*) (*b*) (*c*)

Fig. 7—(*a*) Dark-field images (contrast reversed) from a [112] oriented single crystal aged 3 h at 260 °C with θ' precipitates viewed edge on with dislocations between them. (*b*) Higher magnification showing interface dislocations and small incoherent precipitates. (*c*) SAD confirming the presence of small, incoherent precipitates.

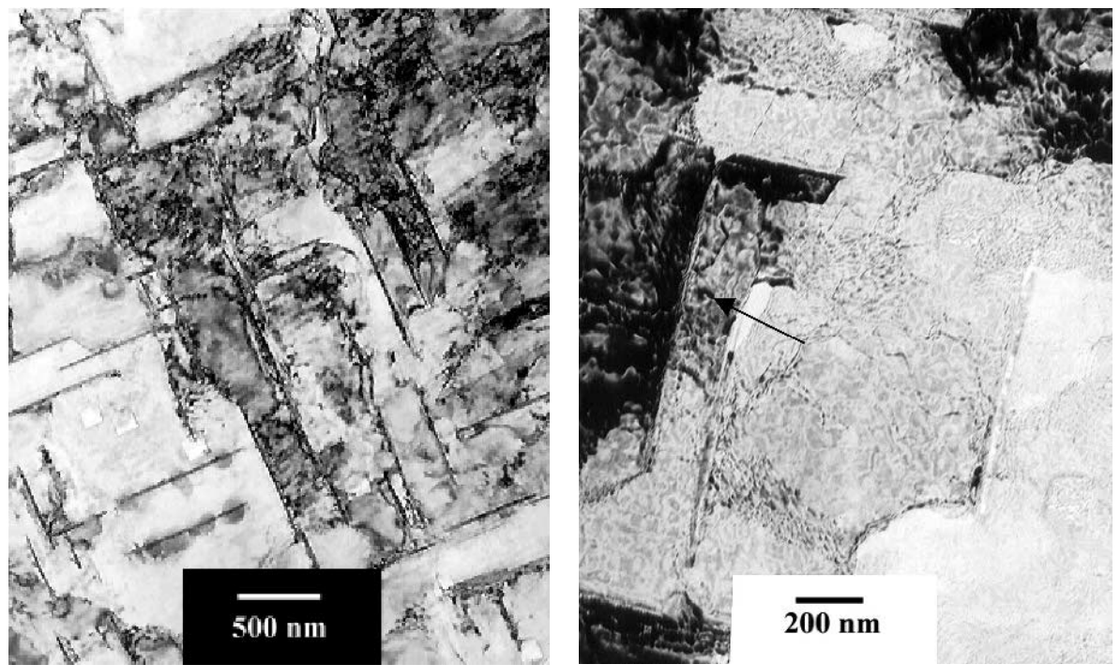

(*a*) (*b*)

Fig. 8—(*a*) TEM images from a [112] single crystal aged at 260 °C for 24 h dark-field images (contrast reversed) showing precipitates and dislocations. (*b*) Higher magnification weak-beam image depicting both θ' and stable θ (shown with arrow) precipitates.

[123] orientations are presented in Figures 10(a) through (c). These results, on Al-4 wt pct Cu, demonstrate the reduction in plastic flow anisotropy between the orientations when precipitates are included in the microstructure. The initial difference between the [111] and [123] orientations for the no-aging case is expected based on the number of slip systems and the Schmid factors. When the samples were aged at 190 °C for 24 hours, the inclusion of precipitates induced an anisotropy offsetting the plastic anisotropy. Aging at 260 °C for 3 hours reduced the plastic flow anisotropy even further, and aging at 260 °C/24 h completely eliminated the flow anisotropy for all orientations (Figures 10(c) and (d)).

To illustrate the role of aging on the stress-strain response, the experimental results for the [112] orientation are summarized in Figures 11(a) and (b). The results for other orientations are similar to the no-aging case exhibiting the highest yield strength followed by a very low hardening. The GP zones in the microstructure initially provide barriers to plastic

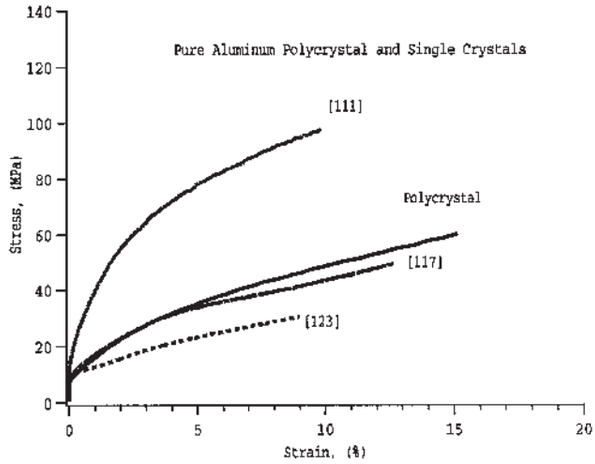

Fig. 9—Comparison of room-temperature stress-strain response of pure aluminum polycrystal and single crystal.

flow resulting in a high yield stress. However, once these zones are sheared, they no longer serve as effective obstacles to dislocation motion and a low hardening rate follows after the onset of yielding. With aging at 190 °C for 3 and 10 hours, the GP zones are eliminated, and the introduction of precipitates provide effective barriers to dislocation motion resulting in increased work hardening. Similarly, for the 260 °C case, the well-developed precipitates produce a higher hardening rate compared to the no-aging case. The hardening rates shown in Figures 12(a) and (b) summarize the higher rate of hardening for the aged cases compared to the solutionized case for all the 190 °C and 260 °C treatments. The hardening rates gradually decrease as relaxation mechanisms occur at high strains with aged and solutionized cases approaching similar levels.

Additional heat treatments were performed at 260 °C for the [111] case to identify the hardening rates. Consistent with other orientations, the yield stress of the sample was lower than the no-aging case (Figure 13). The hardening rates remain

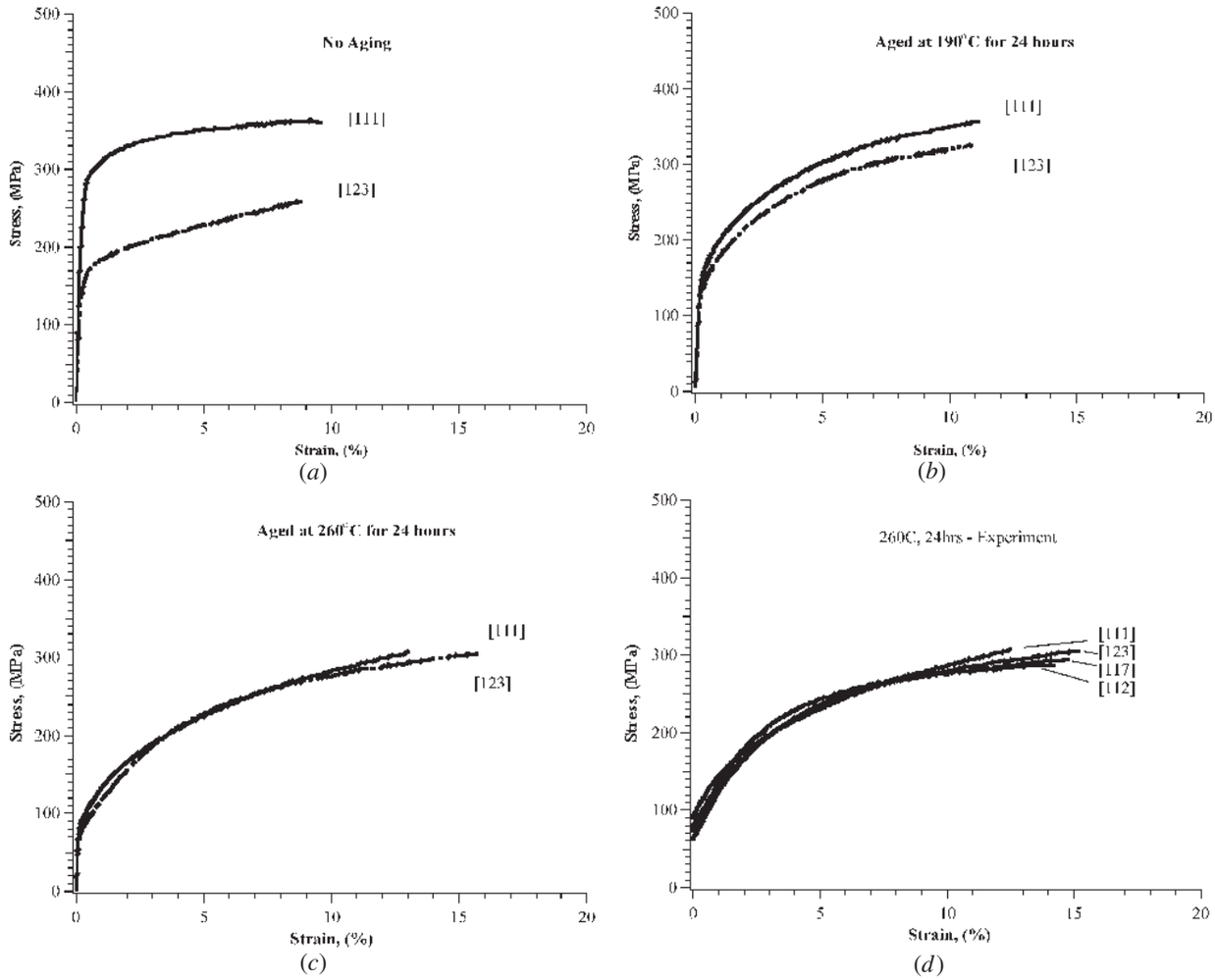

Fig. 10—(*a*) Comparison of [111] and [123] compression stress-strain curves for Al-4 wt pct Cu with no artificial aging showing considerable orientation anisotropy. (*b*) Comparison of [111] and [123] compression stress-strain curves for Al-4 wt pct Cu with aging at 190 °C for 24 h displaying a reduction in orientation anisotropy due to precipitate-induced anisotropy. (*c*) Comparison of [111] and [123] compression stress-strain curves for Al-4 pct Cu with aging at 260 °C for 24 h showing an elimination of anisotropy between the two orientations. (*d*) The reduction of anisotropy with the introduction of precipitates for four orientations of Al-4 wt pct Cu considered in this study.

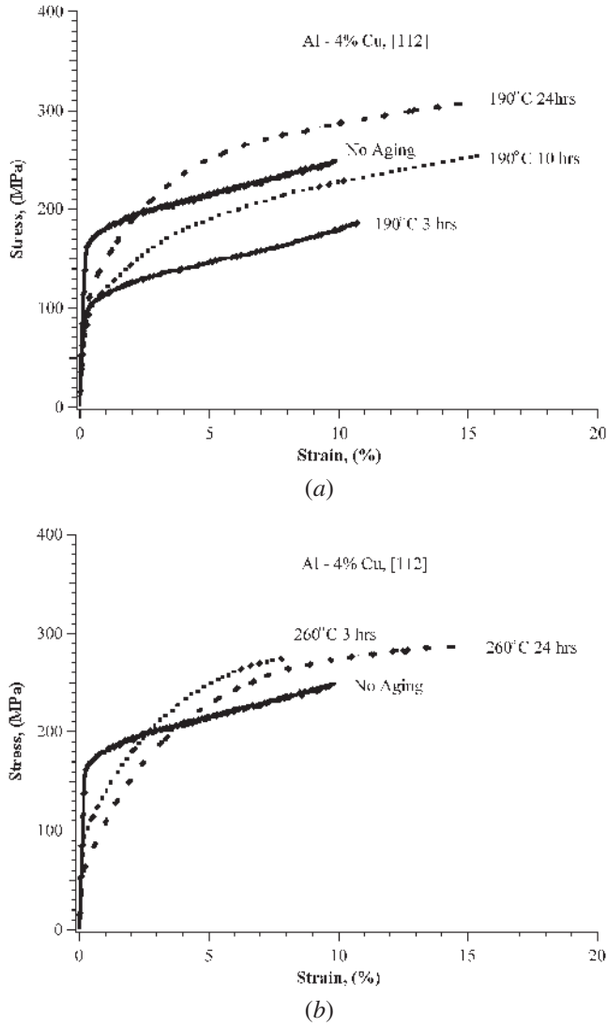

Fig. 11—(*a*) Room-temperature compression stress-strain response of Al-4 wt pct Cu [112] single crystals aged at 190 °C. (*b*) Room-temperature compression stress-strain response of Al-4 wt pct Cu [112] single crystals aged at 260 °C.

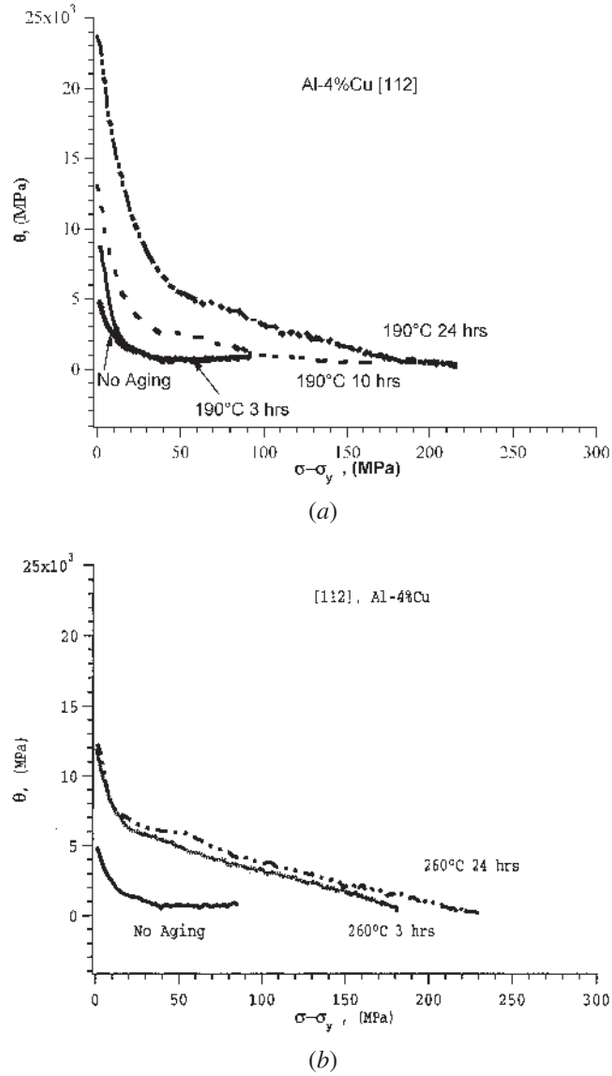

Fig. 12—(*a*) Room-temperature hardening rates of Al-4 wt pct Cu [112] single crystals aged at 190 °C (*b*) Room-temperature hardening rates of Al-4 wt pct Cu [112] single crystals aged at 260 °C.

relatively high in the presence of the precipitates. The hardening rate for [111] aged case exceeded the no-aging case and the hardening rate remained comparatively high attributed to the multiple slip nature of the orientation.

Room-temperature polycrystalline compression experiments are presented in Figures 14(a) and (b). Consistent with all the aged single-crystal samples, the yield strength of the aged polycrystalline samples was less than the samples that did not undergo artificial aging. The curves exhibit a parabolic shape and all treatments resulted in stress-strain curves with high initial hardening rates decreasing gradually after approximately 2 pct strain.

V. SUMMARY OF FINDINGS

The pure aluminum samples exhibited considerable anisotropy as expected from the orientation dependence of the yield strength and the number of active slip systems. This crystal anisotropy was reduced by the introduction of the precipitates in Al-Cu single crystals. The presence of precipitates created anisotropy during plastic deformation that worked in an opposite manner to the crystallographic anisotropy. The strength of the [123] orientation was enhanced more than the [111] orientation resulting in a similar stress-strain curve. The second part of this series of articles will introduce a theory that will predict this effect.

Microstructural analysis was performed by TEM on samples at different aging treatments to determine the precipitate character and active deformation mechanisms. Single crystals were chosen to eliminate the complicating effects of grain boundaries on determining the deformation mechanisms. The influence of orientation and precipitates on the mechanical behavior was also highlighted by single crystals. Compression experiments were used to study the mechanical behavior single and polycrystals of the aluminum and

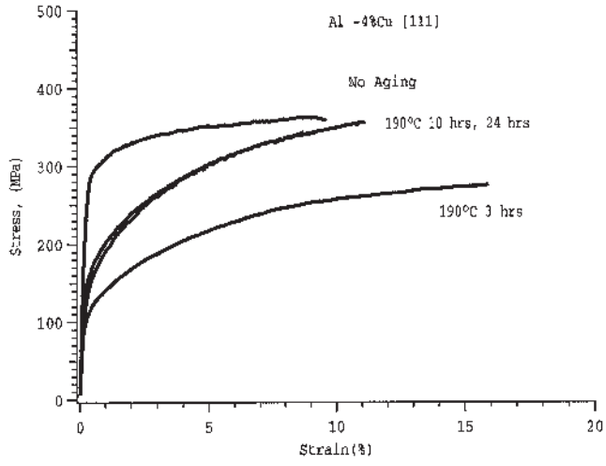

(*a*)

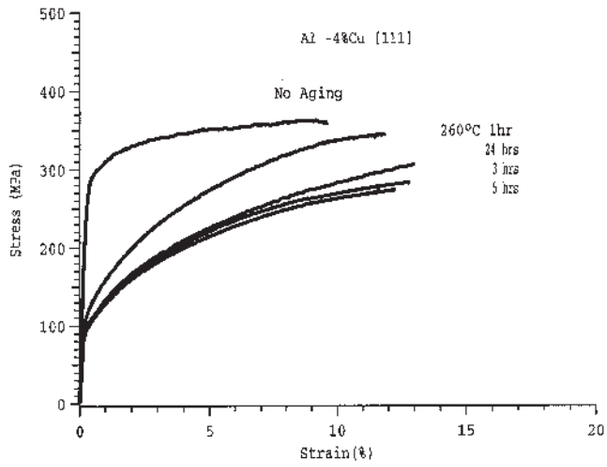

(*b*)

Fig. 13—Room-temperature compression stress-strain response of Al-4 wt pct Cu [111] single crystals aged at (*a*) 190 °C and (*b*) 260 °C.

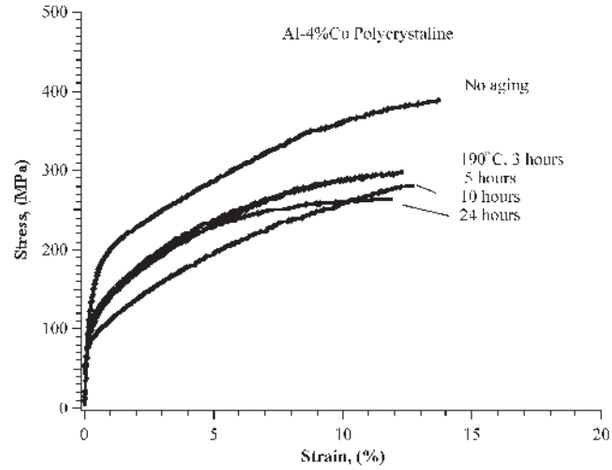

(*a*)

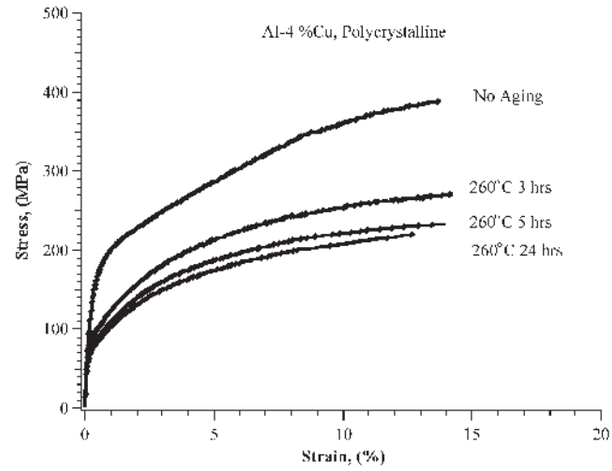

(*b*)

Fig. 14—(*a*) Polycrystalline stress-strain curves of Al-4 pct Cu aged at 190 °C. (*b*) Polycrystalline stress-strain curves of Al-4 pct Cu aged at 260 °C.

aluminum-copper alloy. The different single-crystal orientations clearly demonstrated the changes in precipitate-induced anisotropy by aging.

Pure aluminum was studied so the effects of precipitates on the deformation mechanisms and resulting microstructures could be clearly distinguished, when compared with those of the matrix. Microstructural analysis of the aluminum samples after compression testing showed well-developed dislocation substructures resulting from mobile dislocations interacting with other glissile dislocations and also with forest dislocations that traversed the slip planes. Dislocations were stored in the material through statistical dislocation-dislocation interactions. The correct trends in flow anisotropy due to crystallographic orientation were observed in the single-crystal compression experiments.

The addition of copper as an alloying element significantly changed the deformation mechanisms as precipitates were formed in the matrix at room temperature and by heat treating at 190 °C and 260 °C. The mechanical behavior of the alloy was confirmed to be determined by the character of the precipitates. Coherent GP zones formed at room temperature raised the yield strength but were found to have little impact on the strain hardening behavior. Because the zones were coherent with the matrix, dislocations are known to shear the zones, and they are not effective barriers to further dislocation motion. Elevated temperature aging resulted in the nucleation of semicoherent precipitates. The work hardening of the material increased with aging at 190 °C from 3 to 24 hours. The work hardening rates for samples aged at 260 °C for 3 and 24 hours were similar to one another.

The θ' and θ precipitates were impenetrable obstacles to dislocations resulting in the increased work hardening over the no aging samples. Microstructural analysis revealed that the precipitates not only blocked the dislocations but also confined them to channels between the precipitates forcing them to form energetically unfavorable arrangements. The precipitate spacing also changed with aging, as well as the heterogeneity of the precipitate distribution in the matrix, explaining the changing mechanical behavior with the different heat treatments that resulted in the same precipitate.

ACKNOWLEDGMENTS

The work was partially sponsored by the Ford Motor Company (Dearborn, MI); the Fracture Control Program, University of Illinois; and the National Science Foundation (Grant No. DMR-0313489). The Frederick Seitz Materials Research Laboratory facilities, supported by US Dept. of Energy Grant DEF 02-91ER45439, were utilized in 'texture' portion of the work. The authors acknowledge discussions with C. Tome on the VPSC code modification (Part II), and Professor A. Beaudoin, University of Illinois, Urbana, on texture effects.

REFERENCES

1. R.W.K. Honeycombe: *The Plastic Deformation of Metals,* 2nd ed., Butler & Tanner, Ltd., London, 1984.
2. W.M. Lomer: *Phil. Mag.,* 1951, vol. 42, p. 1327.
3. A.H. Cottrell: *Phil. Mag.,* 1952, vol. 43, p. 645.
4. A.N. Stroh: *Phil. Mag.,* 1956, vol. 1, pp. 489-502.
5. A. Kelly: *Phil. Mag.,* 1956, vol. 1 (9), pp. 835-45.
6. N.J. Petch: *J. Iron Steel Inst.,* 1953, vol. 174, p. 25.
7. R.W. Cahn: *J. Inst. Met.,* 1951, vol. 79, pp. 129-58.
8. T.S. Noggle and J.S. Koehler: *J. Appl. Phys.,* 1957, vol. 28 (1), pp. 53-62.
9. R. Le Hazif and J.-P. Poirer: *Acta Metall.,* 1975, vol. 23, pp. 865-71.
10. P.B. Hirsch, R.W. Horne, and M.J. Whelan: *Phil. Mag.,* 1956, vol. 1, pp. 677-84.
11. A. Mecif, B. Bacroix, and P. Franciosi: *Acta Mater.,* 1997, vol. 45 (1), pp. 371-81.
12. P. Franciosi, M. Berveiller, and A. Zaoui: *Acta Metall.,* 1980, vol. 28 (3), pp. 273-83.
13. D.A. Hughes and A. Godfrey: Sandia National Laboratories Report No. SAND98-8490C, Sandia National Laboratories, 1998.
14. T. Hasegawa and U.F. Kocks: *Acta Metall.,* 1979, vol. 27, pp. 1705-16.
15. E.O. Hall: *Proc. Phys. Soc.,* 1951, vol. 64, p. 747.
16. N.J. Petch: *J. Iron Steel Inst.,* 1953, vol. 174, p. 25.
17. J.E. Bailey, and P.B. Hirsch: *Phil. Mag.,* 1960, vol. 5, pp. 485-97.
18. Z.S. Basinski: *Phil. Mag.,* 1959, vol. 4, pp. 393-432.
19. J.L. Murray: *Int. Met. Rev.,* 1985, vol. 30 (5), pp. 211-33.
20. G.W. Lorimer: *Proc. Precipitation Processes in Solids,* Proc. Symp. sponsored by TMS-AIME Heat Treatment at TMS Meeting, TMS-AIME, Niagara Falls, NY, 1976, pp. 87-97.
21. J.W. Martin: *Micromechanisms in Particle-Hardened Alloys,* Cambridge University Press, Cambridge, United Kingdom, 1980.
22. A. Guinier: *Nature,* 1938, vol. 142, p. 569.
23. G.D. Preston: *Nature,* 1938, vol. 142, p. 570.
24. C. Chiou, H. Herman, and M.E. Fine: *Trans. TMS-AIME,* 1960, vol. 218, pp. 299-307.
25. D. Turnbull, H.S. Rosenbaum, and H.N. Treaftis: *Acta Metall.,* 1960, vol. 8, pp. 277-95.
26. R.G. Baker, D.G. Brandon, and J. Nutting: *Phil. Mag.,* 1959, vol. 4 (48), pp. 1339-45.
27. J.M. Silcock, T.J. Heal, and H.K. Hardy: *J. Inst. Met.,* 1953, vol. 82, pp. 239-48.
28. J.G. Byrne, M.E. Fine, and A. Kelly: *Phil. Mag.,* 1961, vol. 6 (69), pp. 1119-45.
29. J.M. Silcock: *Acta Metall.,* 1959, vol. 8, pp. 589-97.
30. H. Wilsdorf and D. Kuhlmann-Wilsdorf: *Proc. Defects in Crystalline Solids,* The Physical Society, University of Bristol, Bristol, 1954, pp. 175-86.
31. D. Vaughan: *Acta Metall.,* 1968, vol. 16, pp. 563-77.
32. D. Vaughan: *Acta Metall.,* 1970, vol. 18, pp. 183-87.
33. J.D. Boyd and R.B. Nicholson: *Acta Metall.,* 1971, vol. 19, pp. 1379-91.
34. G.C. Weatherly: *Phil. Mag.,* 1968, vol. 17, pp. 791-99.
35. G.C. Weatherly and R.B. Nicholson: *Phil. Mag.,* 1968, vol. 17, pp. 801-31.
36. D. Vaughan: *Phil. Mag.,* 1968, vol. 18, pp. 1305-08.
37. R. Sankaran and C. Laird: *Phil. Mag.,* 1974, vol. 29, pp. 179-215.
38. W.M. Stobbs and G.R. Purdy: *Acta Metall.,* 1978, vol. 26 (7–12), pp. 1069-81.
39. M. Nemoto, N. Morishige, T. Oguchi, and H. Suto: *Trans. Jpn. Inst. Met.,* 1971, vol. 12, pp. 429-33.
40. L.M. Brown, G.R. Woolhouse, and U. Valdrè: *Phil. Mag.,* 1968, vol. 17, pp. 781-89.
41. L.M. Brown and G.R. Woolhouse: *Phil. Mag.,* 1970, vol. 21 (170), pp. 329-45.
42. G.C. Weatherly: *Acta Metall.,* 1971, vol. 19, pp. 181-92.
43. R. Sankaran and C. Laird: *Acta Metall.,* 1974, vol. 22, pp. 957-69.
44. G.C. Weatherly: *Can. Metall. Q.,* 1969, vol. 8 (2), pp. 105-09.
45. A.W. Zhu and E.A. Starke: *Acta Metall. Mater.,* 1999, vol. 47 (11), pp. 3263-69.
46. H. Hargarter, M.T., Lyttle, and E.A. Starke: *Mater. Sci. Eng.,* 1998, vol. A257, pp. 87-99.
47. B. Skrotzki, G.J. Shiflet, and E.A. Starke: *Metall. Mater. Trans. A,* 1996, vol. 27A, pp. 3431-44.
48. W.F. Hosford and S.P. Agrawal: *Metall. Mater. Trans. A,* 1975, vol. 6A, pp. 487-91.
49. A.W. Zhu, J. Chen, and E.A. Starke Jr.,: *Acta Mater.,* 2000, vol. 48, pp. 2239-46.
50. V.B. Nileshwar: *J. Inst. Met.,* 1963–64, vol. 92, pp. 241-45.
51. D. Driver and P. Barrand: *Phil. Mag.,* 1966, vol. 14, pp. 657-65.
52. G. Thomas and M.J. Whelan: *Phil. Mag.,* 1961, vol. 6 (69), pp. 1103-14.
53. C. Laird and H.I. Aaranson: *Acta Metall.,* 1966, vol. 14, pp. 171-85.
54. T.J. Smith: Master's Thesis, University of Illinois at Urbana–Champaign, Urbana, 1998.
55. T.J. Smith, H.J. Maier, H. Sehitoglu, E. Fleury, and J. Allison: *Metall. Mater. Trans. A,* 1999, vol. 30A, pp. 133-46.
56. H.K. Hardy: *J. Inst. Met.,* 1951, vol. 79, pp. 321-69.
57. H.K. Hardy: *J. Inst. Met.,* 1953, vol. 82, pp. 236-38.
58. A. Abel and R.K. Ham: *Acta Metall.,* 1966, vol. 14, pp. 1489-94.
59. G.D. Moan and J.D. Embury: *Acta Metall.,* 1979, vol. 27, pp. 903-14.
60. K.C. Russell and M.F. Ashby: *Acta Metall.,* 1970, vol. 18, pp. 891-901.
61. R.J. Price and A. Kelly: *Acta Metall.,* 1964, vol. 12, pp. 159-69.
62. D.V. Wilson: *Acta Metall.,* 1965, vol. 13, pp. 807-14.
63. V. Gerold and H. Haberkorn: *Phys. State Solids,* 1966, vol. 16, pp. 675-84.
64. M.F. Ashby: *Phil. Mag.,* 1970, vol. 21, pp. 399-424.
65. S. Koda K. Matsuura, and S. Takahashi: *J. Inst. Met.,* 1962, vol. 91, pp. 229-34.
66. S.N. Buckley and K.M. Entwistle: *Acta Metall.,* 1956, vol. 4, pp. 352-61.
67. F. Barlat and A.K. Vasudévan: *Acta Metall. Mater.,* 1991, vol. 39 (3), pp. 391-400.
68. T.J. Foglesong: Ph.D. Thesis, University of Illinois at Urbana–Champaign, Urbanan IL, 2001.
69. J.S. Kallend, U.F. Kocks, A.D. Rollet, and H.R. Wenk: *Mater. Sci. Eng.,* 1991, vol. A132, (1–2), pp. 1-11.
70. T. Tabata, S. Yamanaka, and H. Fujita: *Acta Metall.,* 1978, vol. 26, pp. 405-11.
71. T. Tabata, H. Fujita, M.-A. Hiraoka, and S. Miyake: *Phil. Mag. A: Phys. Condensed Matter Defects Mech. Prop.,* 1982, 46 (5), pp. 801-16.
72. C. Calabrese and C. Laird: *Mater. Sci. Eng.,* 1974, vol. 13, pp. 159-74.